Journal of Applied Physics ARTICLE pubs.aip.org/aip/jap

Temperature dependence of deep level positions and capture cross sections in vanadium-doped 4H-SiC

Cite as: J. Appl. Phys. **137**, 175707 (2025); doi: 10.1063/5.0256960
Submitted: 8 January 2025 · Accepted: 15 April 2025 ·
Published Online: 5 May 2025

Yuxuan Lan,[1] Bo Peng,[1,a)] Yutian Wang,[1,b)] Hao Yuan,[1] Jichao Hu,[2] Linpeng Dong,[3] Hui Guo,[1] and Yuming Zhang[1]

AFFILIATIONS

[1]School of Microelectronics, Key Laboratory of Wide Band-Gap Semiconductor Materials and Devices, Xidian University, Xi'an 710071, China
[2]Department of Electronic Engineering, Xi'an University of Technology, Xi'an 710048, China
[3]Shaanxi Province Key Laboratory of Thin Films Technology and Optical Test, Xi'an Technological University, Xi'an 710032, China

[a)]**Author to whom correspondence should be addressed:** boopeng@xidian.edu.cn
[b)]**Electronic mail:** ytwang@xidian.edu.cn

ABSTRACT

4H-SiC has emerged as a crucial semiconductor material for power electronic devices due to its superior physical properties, including high breakdown field, electron saturation drift velocity, and thermal conductivity. Vanadium, an amphoteric transition metal impurity and intra-transition color center in 4H-SiC, plays a vital role through compensation doping to prepare semi-insulating substrates, with applications in microwave power and quantum devices. Using density functional theory with screened hybrid functionals and Heyd, Scuseria, and Ernzerhof + V_w corrections, we investigated temperature-dependent behavior of V acceptor levels and capture cross sections to interpret deep-level transient spectroscopy (DLTS) signals. Our research reveals that at 800 K, the $V_{Si}(0/-)$ transition level decreases by approximately 0.07 eV compared to 0 K, while electron capture cross sections increase by more than 1000 times their room temperature value. Considering the intra-transition excited states of V ions, we predicted additional transition levels and temperature-dependent capture cross sections. The theoretically predicted $0/-$ and $0^*/-^*$ levels align well with two DLTS peaks: E1 at 425 K (corresponding to an activation energy of 0.85 eV) and E2 at 660 K (corresponding to an activation energy of 1.15 eV). We calculated entropy factors from theoretical-apparent capture cross section discrepancies. This research enhances understanding of DLTS results for vanadium impurities in 4H-SiC, helping establish temperature dependence of trap energy levels and Shockley–Read–Hall recombination rates, benefiting high-temperature power device modeling and photoconductive switch simulations under specific conditions.

I. INTRODUCTION

As a prominent representative of wide bandgap semiconductors, silicon carbide (SiC) exhibits superior characteristics including high breakdown electric field, high thermal conductivity, high electron saturation drift velocity, strong radiation resistance, and high chemical stability. These properties establish SiC as a crucial semiconductor material for the fabrication of high-performance power devices designed for applications in power electronic systems, as well as for high-temperature and radiation-resistant operations.[1,2]

Vanadium is an amphoteric transition metal impurity in 4H-SiC that can produce thermally stable deep levels.[3–6] Consequently, it is commonly used to compensate for active donor and acceptor impurities in the preparation of semi-insulating substrates or epitaxial layers for applications in microwave power devices. Recent studies have revealed that vanadium-compensated semi-insulating (VCSI) 4H-SiC is an ideal candidate material for photoconductive semiconductor switches (PCSSs).[7,8] In this device, vanadium acts as a source for free electrons or holes, facilitating

sub-bandgap photon-induced electron transitions to the conduction band or hole transitions to the valence band. This process determines the photoconductive properties of the device and demonstrates a relatively short carrier recombination lifetime of less than 100 ps.[9] Furthermore, recent research has indicated that the long lifetime intra-transition color center characteristics of V impurities in 4H-SiC within the telecom wavelength range, as well as the large hyperfine Hilbert space provided by their intrinsic nuclear spin, demonstrate significant potential for applications in emerging quantum technologies such as single-photon emission diodes, solid-state quantum registers, and photon-spin interfaces.[10–14]

The implementation of silicon carbide power and quantum devices described above is fundamentally based on a precise understanding of the optical and electrical properties of V impurity levels within the bandgap. This includes comprehension of impurity-band transitions in various charge states, intra-3*d* shell transitions, and recombination processes. To characterize the optical and electrical properties of vanadium impurities, several analytical techniques are employed. These include photoluminescence spectroscopy (PL),[3,14,15] deep level transient spectroscopy (DLTS),[16–18] and electron spin resonance spectroscopy (ESR).[6,19–21]

First-principles calculations based on density functional theory have provided significant assistance in interpreting the experimental results. For example, the calculation of thermodynamic transition levels (charge transition levels) explains the deep level positions measured by DLTS.[22,23] The delta-self-consistent-field method, through calculations of zero-phonon lines (ZPLs), phonon sidebands, Huang–Rhys factors, and spectral functions, is used to interpret temperature and time-dependent PL measurements related to inner transitions associated with neutral charge state substitutional V^{4+}.[14] The calculation of zero-field splitting, electronic g-tensors, and hyperfine coupling constants for V^{3+} acceptors at different Si sites is used to explain results obtained through ESR experiments.[19]

Throughout the research process from early stages to the present, DLTS has maintained a prominent position in the study of vanadium impurities in 4H-SiC, particularly in the characterization of acceptor levels. Early characterization of V-doped samples grown using different techniques revealed levels located 0.80–0.97 eV below the conduction band minimum (CBM).[5,24–26] Recently, a current-mode DLTS (I-DLTS) technique, suitable for characterizing high-resistivity samples with high trap concentrations, identified a deep level with an activation energy of 0.87 eV, attributed to V substituting Si defects.[17] Standard DLTS measurements have also observed deep centers at CBM − 0.97 eV in high-quality V-doped epitaxial layers grown by chemical vapor deposition (CVD) methods, further confirming its correspondence to the $V^{4+/3+}$ acceptor level.[18] Additionally, DLTS peaks corresponding to vanadium centers have been observed in V ion-implanted epitaxial layers.[16] Despite the long-standing research on this issue, with the development of theoretical calculations related to the interpretation of DLTS characterization, we have identified three problems in the theoretical study of V deep levels in 4H-SiC.

First, the DLTS peaks associated with the V acceptor level were observed above 400 K. In this case, using the peak center position as input for traditional Arrhenius fitting of the emission rate results in an activation energy that deviates from the ionization energy of the defect at 0 K. Wickramaratne *et al.*[27] pointed out that this phenomenon is mainly caused by the temperature dependence of the ionization energy and capture cross section in the following equation:

$$e_n(T) = \sigma_n(T)\langle v_{th,n}(T)\rangle N_c(T) X_n \exp\left(-\frac{\Delta E_i(T)}{k_B T}\right). \quad (1)$$

This expression, widely employed to describe the temperature dependence of the emission rate determined from DLTS measurements, is derived under equilibrium conditions, where the principle of detailed balance ensures that the rate of electron capture into the defect level equals the rate of electron emission into the conduction band. For the V acceptor level, where $v_{th,n}(T)$ is the average thermal velocity of electrons in the conduction band, $N_c(T)$ is the effective density of states of the conduction band, X_n is the entropy factor, and $\Delta E_i(T)$ is the ionization energy of the defect, representing the energy difference between the defect level and the CBM. Therefore, to correctly use density functional theory to interpret DLTS experimental results, it is necessary to consider the temperature dependence of the ionization energy and capture cross section.[27,28]

To study the temperature dependence of the ionization energy, one first needs to compute the thermodynamic transition levels in the ground state, i.e., at 0 K. Subsequently, the temperature dependence of the thermodynamic transition levels, or ionization energies, can be determined by considering the temperature-induced changes in the band edges and the differences in vibrational free energy between defects in specific charge states.[27] More importantly, although the variation of ionization energy with temperature might be falling within the uncertainty range of the activation energy measured by DLTS, i.e., ∼0.1 eV, its impact on the capture cross section cannot be neglected.

To investigate the temperature dependence of capture cross sections, we adopt the multiphonon-assisted nonradiative capture rate calculation method based on static coupling, as described in Ref. 29. This approach incorporates a more accurate calculation by accounting for the influence of temperature-dependent ionization energy on the capture cross sections. Furthermore, the variation of capture cross sections with temperature can provide deeper insights into the analysis of DLTS experimental results. In standard DLTS procedures, the apparent capture cross section is typically determined from the intersection of the $\ln(v_{th,n}(T)N_c(T)e_n^{-1})$ vs 1/T curve. During this fitting process, the capture cross section is often assumed to be temperature-independent and includes the product with the entropy factor described in Eq. (1). The entropy factor can be expressed as $X_T = \exp(\Delta S/k)$, where the reaction entropy ΔS arises from the difference between the defect ionization energy and the Gibbs free energy during the carrier emission process. Experimentally, the entropy factor can be determined by measuring the temperature dependence of carrier concentration or by fitting multiple spectra obtained with different filling-pulse lengths simultaneously.[30,31] However, in the former case, precise measurements of temperature-dependent carrier concentrations are challenging for highly resistive 4H-SiC samples with high V doping due to their typically low carrier densities. For the latter, it essentially relies on multi-parameter fitting, which introduces uncertainties, especially for specific defects such as ON2 in 4H-SiC, where variations in the

entropy factor within a certain range have been shown to have minimal impact on the fit quality.[31] Additionally, direct measurements of the temperature dependence of capture cross sections by varying the filling-pulse widths face issues such as repeated measurements at high temperatures, which have been demonstrated to potentially affect the barrier height of Schottky contacts in the sample.[32] Therefore, isolating the entropy factor from the apparent capture cross section derived from Arrhenius fitting remains challenging. To date, reported entropy factor values ΔS for defects in 4H-SiC are limited. For example, ΔS for the carbon vacancy has been reported to be approximately $5k_B$ (where k_B is the Boltzmann constant),[33] while values related to shallow and deep boron impurities range from 0.1 to $6k_B$.[34] Further investigations are required to determine ΔS for defect levels associated with V impurities. In conclusion, measurements of the capture cross sections for V impurity levels at different temperatures using DLTS are subject to uncertainties. First-principles calculations are thus essential for guiding the interpretation of experimental results.

In addition to temperature-induced shifts in transition level positions, the inner-shell excited states of transition metal impurities in different charge states may introduce new donor or acceptor levels within the bandgap of wide-bandgap semiconductors. Wickramaratne *et al.*[35] proposed this phenomenon in Fe-doped GaN, discussing its potential impact on carrier recombination pathways and explaining why midgap Fe impurity levels can act as efficient Shockley–Read–Hall (SRH) recombination centers. For V impurities in 4H-SiC, several studies have investigated intra-band transitions associated with neutral charge states, as evidenced by the α-lines and β-lines observed in the infrared region of low-temperature photoluminescence spectra.[3,14] For the V^{3+} acceptor level, reports have documented doublet ZPLs around 5400 cm^{-1} attributed to the $3A^2 \rightarrow 3T^2$ transition, as well as ZPLs near 7000 cm^{-1}, attributed to higher excited states.[24] These findings have been preliminarily confirmed by recent density functional theory (DFT) total energy calculations and photo-EPR measurements by von Bardeleben *et al.*[19] However, the thermal transition levels corresponding to these inner-shell excited states in V-doped 4H-SiC systems have not yet been thoroughly investigated. It remains unclear whether these levels could influence the experimentally measured DLTS signals. Therefore, theoretical calculations are necessary to further explore this phenomenon. Such studies could also help determine the capture cross sections corresponding to transition levels associated with these excited states.

Regarding the three issues raised above concerning the interpretation of DLTS signals in V-doped 4H-SiC, we have conducted an in-depth investigation using density functional theory on three aspects in this work: the temperature dependence of V thermodynamic transition energy levels, the temperature dependence of capture cross sections, and the new transition energy levels introduced by internal excitation states along with their corresponding capture cross sections. These aspects were overlooked in previous studies. We first use DFT calculations to investigate the temperature dependence of acceptor transition levels associated with V dopants in 4H-SiC. Based on these calculations, we evaluate the variation of capture cross sections with temperature. Next, we examine the transition levels introduced by excited states related to intra-3*d* shell transitions of neutral and negatively charged V^{4+} and V^{3+} ions, as well as their corresponding capture cross sections. Finally, we characterize semi-insulating 4H-SiC samples doped with V using current-mode DLTS. By interpreting the Arrhenius fitting results with the aid of theoretical calculations, we propose a new hypothesis for the origin of one observed peak. The research on thermal and optical excitation of thermodynamic transition energy levels helps to develop a deeper understanding of DLTS results related to V impurities in 4H-SiC materials, thereby contributing to the field of electrical properties research of deep-level impurities in 4H-SiC. Based on this study, we can further derive the patterns of temperature dependence for V impurity trap energy levels and their associated SRH recombination rates, which is beneficial for improving high-temperature models of relevant power and optoelectronic devices. Particularly for photoconductive switch devices, this work provides a theoretical foundation for simulating their operation and understanding their working mechanisms under specific operating conditions, such as above room temperature environments and under 532 nm wavelength optical excitation.

II. MATERIALS AND METHODS

A. Computational methods

First-principles calculations were performed based on density functional theory using the plane wave material simulation package PWmat.[36] The SG15 version of optimized norm-conserving Vanderbilt pseudopotentials[37] was used for the relevant elements. The valence electron configurations for C, Si, and V were $2s^2 2p^2$, $3s^2 3p^2$, and $3s^2 3p^6 4s^2 3d^3$, respectively. Structure relaxation and self-consistent calculations utilized the screened hybrid functional developed by Heyd, Scuseria, and Ernzerhof (HSE)[38] mixed with the exchange potential of Perdew, Burke, and Ernzerhof (PBE).[39] The mixing parameter α and the screening parameter ω were set to 0.25 and 0.2 $Å^{-1}$, respectively.

When performing calculations on the primitive unit cell containing eight atoms, the plane wave basis set was employed with a kinetic energy cutoff of 60 Ry. The maximum residual force on each atom was constrained to be less than 0.005 eV/Å, and the convergence criterion for the total energy in self-consistent iterations was set to 1×10^{-5} eV. The relaxed lattice parameters of the primitive cell were found to be a = 3.079 Å, c = 10.071 Å, which agree well with the experimental values reported in the literature (a = 3.08 Å, c = 10.08 Å).[1] Using the method provided in Ref. 40 to determine the high-symmetry points in the Brillouin zone, the calculated fundamental bandgap of 4H-SiC was 3.23 eV, which is in excellent agreement with the experimental value of 3.26 eV.[1]

For calculations involving the inclusion of V dopants, a supercell consisting of 200 atoms was constructed as a $5 \times 5 \times 1$ repetition of the primitive cell. For the self-consistent calculations of the supercell, convergence tests revealed that increasing the cutoff energy to 70 Ry resulted in a variation in transition energy levels of about 0.01 eV. A single Γ-point was used for sampling the Brillouin zone. The self-consistent iterations for charge density were carried out using the full-band conjugate gradient method. During the relaxation of the supercell structure, the maximum residual force on each atom was constrained to be less than 0.02 eV/Å, while the

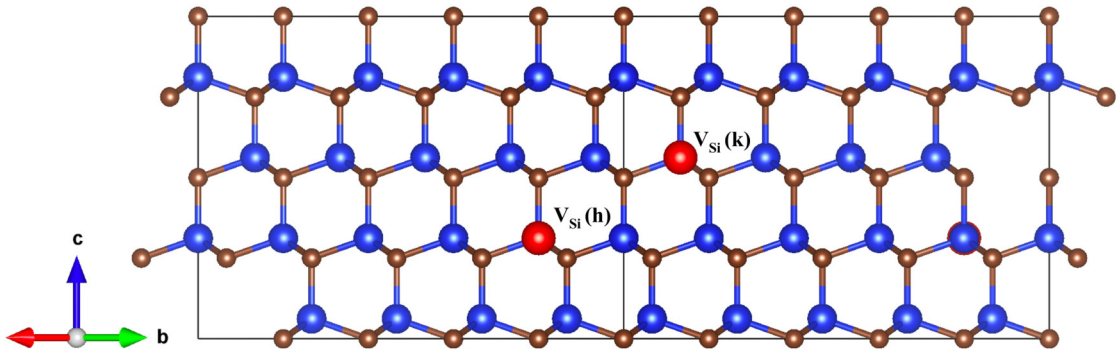

FIG. 1. Schematic representation of V substitutional impurities in a 200-atom 4H-SiC supercell. The V impurities at hexagonal and cubic Si sublattice sites are labeled as V_{Si}(h) and V_{Si}(k), respectively, and are depicted as red solid spheres. Silicon atoms are represented by blue solid spheres, while carbon atoms are shown as brown solid spheres.

total energy convergence criterion in the self-consistent iterations was maintained at 1×10^{-5} eV.

For Si and C in 4H-SiC, due to differences in the structures of their immediate neighbors, there are hexagonal sites and cubic sites with different surroundings, which are denoted as *h* and *k*, respectively. In this study, we focus on the experimentally well-established substitutional V defect at the Si lattice site and label the substitutional hexagonal and cubic Si sublattice as V_{Si}(h) and V_{Si}(k), respectively, as shown in Fig. 1. Furthermore, it should be noted that the charge-state notation of transition levels used in first-principles calculations corresponds to the oxidation-state notation commonly adopted in experimental literature. For example, V(0/−) is equivalent to $V^{4+/3+}$, both representing a neutral V ion capturing one conduction band electron and transitioning to a negatively charged V ion.

For calculations involving vanadium-doped systems, spin polarization is considered to improve the accuracy of the total energy. This approach has been validated in previous studies on various materials related to vanadium and other transition metals.[41,42] The corrections were made using the HSE + V_w method proposed by Ivády *et al.*,[43] which is analogous to the DFT + U approach, introduces an orbital-dependent correction term, $V_w = w(1/2 - n)$, where the specific value of w depends on the charge state and lattice site of the vanadium atom. The aim of this approach is to ensure that the system satisfies the generalized Koopmans theorem, which will be elaborated upon in the section discussing transition level calculations.

When calculating the formation energy, to eliminate the artificial Coulomb interactions between charged defects caused by the periodic boundary conditions of the supercell model, we adopted the image charge correction method based on self-consistent charge density recently proposed by Suo *et al.*[44] This method has been successfully extended in our previous research to transition-metal-doped wide-bandgap semiconductors.[45]

B. Experimental details

We used 10×10 mm^2 square samples obtained by laser cutting from a commercially available 4-in. vanadium-doped semi-insulating substrate produced by SICC Co., Ltd. The substrate had a nitrogen donor concentration of [N] = 2×10^{17} cm^{-3} and a vanadium donor concentration of [V] = 1×10^{17} cm^{-3}. For DLTS testing, we first deposited a 6 mm × 6 mm × 300 nm Ni layer on the C-face and performed rapid thermal annealing at 1000 °C for 5 min in a nitrogen atmosphere. Subsequently, Ti/Al (120 nm/200 nm) was deposited. Using a shadow mask, a 2 mm diameter Ni/Ti/Au (300 nm/120 nm/200 nm) layer was deposited on the Si-face to form Schottky contacts.

Current-mode DLTS measurement was performed using a PhysTech FT-1030 HERA-DLTS system. Compared to the standard capacitance-mode DLTS, I-DLTS has been demonstrated to be effective for testing high-resistivity SiC samples, overcoming the limitation that the standard mode requires the trap concentration to be less than 10% of the net donor (or acceptor) concentration.[17] During the measurements, the C-face electrode of the sample was in contact with a gold plate mounted on the chip carrier, while the Si-face electrode was contacted with a probe. The time window was set to 9.73 ms, the filling pulse width was 3 ms, the reverse bias was −15 V, and the pulse voltage was 6 V.

Our set reverse bias voltage is close to the corresponding reverse bias voltage used in the literature when making Schottky contacts with the same Ni.[31] Based on the Fermi level position calculated from resistivity testing (CBM −0.9 eV, as shown in Sec. III) and the typical Schottky barrier height formed between Ni and n-type 4H-SiC (1.7 eV), the built-in potential of the space charge region can be determined to be approximately 0.8 eV. With this foundation, by incorporating the reverse bias voltage, the concentration of ionized N impurities, and the dielectric constant of 4H-SiC, we can calculate that the width of the space charge region under reverse bias is about 0.4 μm. For a uniformly doped substrate, V impurities can be considered uniformly distributed within this width (thickness). Based on the determined reverse bias voltage, we tested different pulse voltages lower than the reverse bias voltage and further observed the intensity of the corresponding DLTS signals. We found that when the pulse voltage is 6 V, the corresponding signal peak is most significant, therefore we finally selected these test conditions.

III. RESULTS AND DISCUSSION

A. Thermodynamic transition energy level at 0 K

1. Transition levels in the ground state

The thermodynamic transition levels at the ground state, i.e., the ionization energies at 0 K, can be calculated using Eq. (2),[44,46]

$$\varepsilon(q/q') = \frac{\Delta H_f(X, q)_{E_F=0} - \Delta H_f(X, q')_{E_F=0}}{q' - q}, \quad (2)$$

where $\Delta H_f(X, q)_{E_F=0}$ represents the formation energy of defect X in charge state q with the Fermi level set to 0. It can be determined using Eq. (3),[46,47]

$$\Delta H_f(X, q) = \{E(X, q) + E_{\text{corr}}(X, q)\} - E(\text{host}) - \sum_i n_i \mu_i + q(E_F + E_{\text{VBM}} + \Delta V), \quad (3)$$

where $E(X, q)$ is the total energy of the supercell containing the defect X in charge state q. $E_{corr}(X, q)$ is the correction term accounting for finite-size effects (e.g., image charge correction). $E(host)$ is the total energy of the corresponding perfect supercell (without defects). n_i is an integer representing the number of atoms of species i added ($n_i > 0$) or removed ($n_i < 0$) from the perfect supercell to create the defect. μ_i is the chemical potential of atomic species i, which is referenced to the total energy E_i of the elemental phase of that atom. E_F is the Fermi level, which is referenced to the valence band maximum (VBM) energy E_{VBM} for this calculation. ΔV is the potential alignment term accounting for differences in the reference potential between the host and defect supercell.

We can determine the chemical potential boundaries in Eq. (3) based on the growth conditions. In the Si-rich limit, $\mu_{Si} = 0$. To maintain the stability of the 4H-SiC phase, we require $\mu_{Si} + \mu_C = \Delta H_f$ (SiC), where ΔH_f (SiC) refers to the formation energy of 4H-SiC. In this calculation, the value obtained is −0.499 eV, which is close to previous calculations but larger than the experimental value of −0.73 eV.[48,49] Similarly, in the C-rich limit, we set $\mu_C = 0$. Furthermore, for the V-doped system, two additional constraints should be considered. First, to avoid precipitation of elemental vanadium, we require $\mu_V \leq 0$. Second, to prevent phase separation into competing transition metal compounds, we require $x\mu_V + y\mu_{Si} \leq \Delta H_f$ (V_xSi_y) and $p\mu_V + q\mu_C \leq \Delta H_f$ (V_pC_q), where ΔH_f (V_xSi_y) and ΔH_f (V_pC_q) denote the formation energies of experimentally observable vanadium silicides and carbides, respectively.[50] In this study, we consider V_3Si, VSi_2, V_6Si_5, V_2C, and VC.

As mentioned in Sec. II, in the total energy calculations, the HSE + V_w method was employed for corrections,[43] where different strength parameters w were selected for V impurities in various charged states to ensure that the system satisfies the generalized Koopmans' theorem. This implies that the difference in total energy ΔE_{SCF} between systems with total electron numbers N and N-1 should approximately equal the value of the highest occupied molecular orbital (HOMO) energy level E_{KSHOMO} for the system with N electrons, i.e., $E_{NK} = \Delta E_{SCF} - E_{KSHOMO} \approx 0$. For V_{Si}(h), we chose w = −2.2 eV and w = −5.5 eV to calculate the positions of the (0/−) and (0/+) transition levels within the bandgap, respectively. For V_{Si}(k), $w = -4.2$ eV and $w = -5.0$ eV were selected for the (0/−) and (0/+) transition levels, respectively. When comparing the formation energies of V substitutional impurities in different configurations to determine their relative stability, a common screening parameter w_c was required. In this study, we adopted $w_c = -3.2$ eV, derived from the average of the w values corresponding to neutral substitutional V impurities at two different Si sites. The formation energies for other charged states of the substitutional impurities could then be determined based on the formation energies of the two neutral states and the positions of the (−/0) and (0/+) transition levels within the bandgap. The formation energies for the two neutral states obtained in this study were lower than those recently obtained using the GGA + U method,[51] where it was 4.05 eV. Based on the equation $n(X, 0) = N_{\text{site}}\, g_0 \exp(-\frac{\Delta H_f(X, q)}{k_B T})$ (where N_{site} is the number of lattice sites per unit volume that defect X can occupy, and g_0 is the degeneracy factor that corresponds to the number of possible electron configurations) and the formation energies under C-rich conditions provided in Fig. 2, the concentration of neutral V impurities at the typical epitaxial layer growth temperature (1900 K) is calculated to be on the order of 10^{14} cm^{-3}. However, it is evident that this concentration estimation is underestimated, which is most likely caused by the deviation introduced when using the average value of w to calculate the formation energy.

The orange and purple solid lines in Figs. 2(a) and 2(b) show the formation energies of V impurities at two types of Si sites in different charge states as a function of the Fermi level under Si-rich and C-rich limits, respectively. First, it is observed that, under both Si-rich and C-rich growth conditions, the formation energy of neutral substitutional V_{Si}(h) at the hexagonal Si sublattice site (3.79 eV under Si-rich and 2.92 eV under C-rich conditions) is lower than that of neutral substitutional V_{Si}(k) at the cubic Si sublattice site (3.90 eV under Si-rich and 3.03 eV under C-rich conditions). This indicates that V is more likely to substitute at hexagonal Si sites, consistent with the conclusion in Ref. 52, which attributes this preference to the larger nearest-neighbor atomic spacing and lower symmetry of hexagonal sites, making them energetically more favorable. Second, compared to Si-rich conditions, the lower formation energies of V_{Si}(h) and V_{Si}(k) under C-rich conditions reveal that V substitutional doping at Si sites is more easily achieved under C-rich conditions. This is consistent with the recent experimental findings for the growth of high-resistivity epitaxial layers of V-doped 4H-SiC, as reported in Refs. 4 and 53, which show that the V concentration increases with increasing C/Si ratio due to the site competition principle. Finally, for V_{Si} at both lattice sites, the positively charged state is more stable than the neutral state when the Fermi level is near the VBM, whereas the negatively charged state is more stable when the Fermi level is closer to the CBM. The calculated thermodynamic transition levels of V_{Si}(h) and V_{Si}(k) are located at CBM of − 0.91 eV and CBM of − 0.84 eV for the (0/−) transition, and at VBM + 1.23 eV and VBM + 1.21 eV for the (+/0) transition, respectively.

For the semi-insulating samples used in this study, the resistivity is measured to be $1 \times 10^{12}\ \Omega$ cm. Due to V-compensated n-type doping, the majority carriers are electrons, and the Fermi level of the system is expected to be positioned at CBM − 0.9 eV.

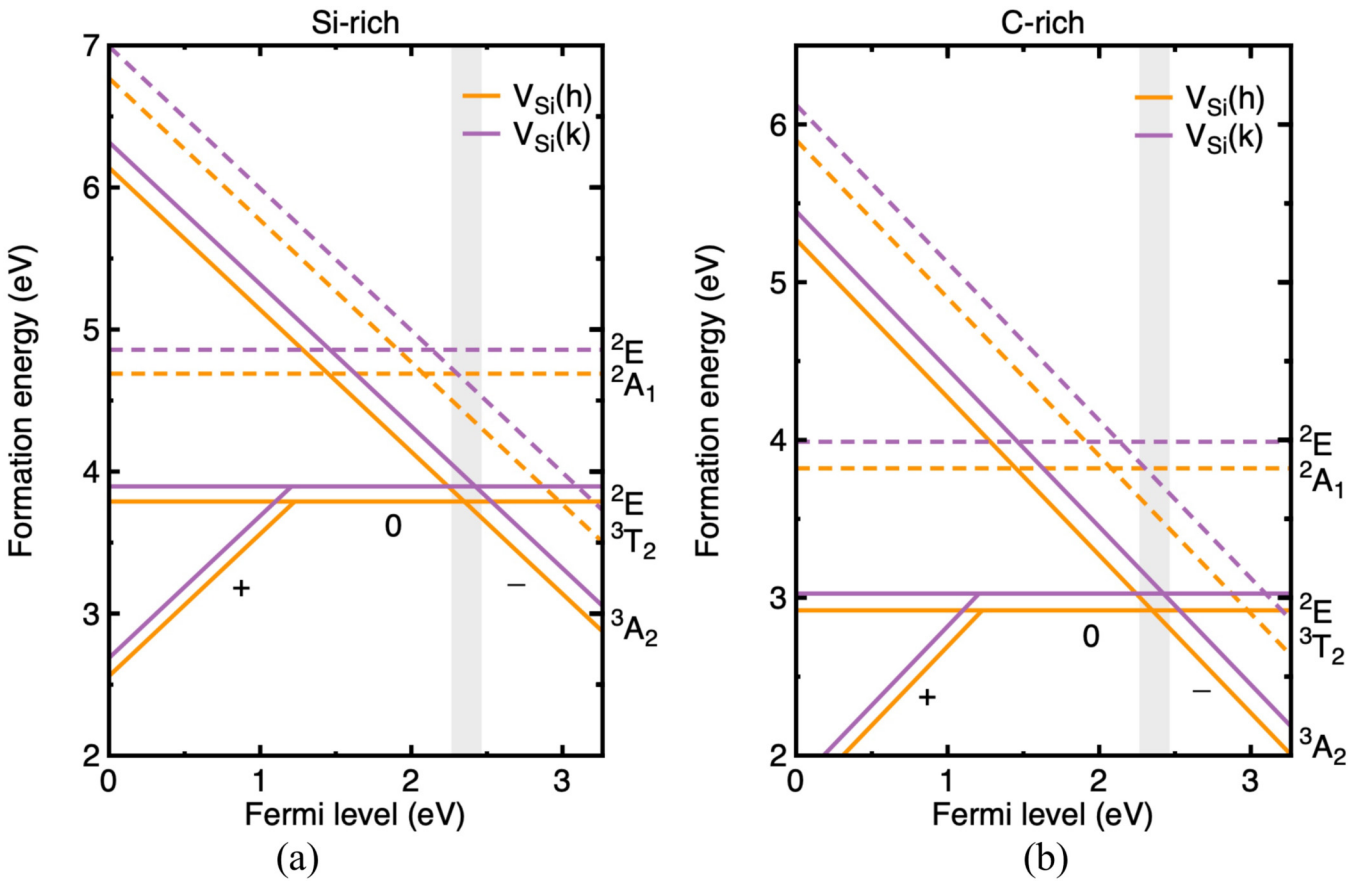

FIG. 2. Formation energies of V impurities at different Si sites in 4H-SiC as a function of Fermi level. Solid orange and purple lines represent the ground state formation energies under Si-rich (a) and C-rich (b) conditions, respectively, for V impurities at two different Si lattice sites in various charge states. Dashed lines indicate the formation energies associated with intra-3*d* shell excited states. The labels distinguishing different ground and excited states are positioned along the right vertical axis.

Considering the errors inherent DFT calculations and the uncertainties in high-resistivity measurements, we may define the range of the Fermi level as CBM $-$ 0.9 $\pm$ 0.1 eV, as indicated by the gray area in Fig. 2. It can be observed that under these conditions, $V_{Si}(h)$ and $V_{Si}(k)$ could exist either in the neutral state V^{4+} or carry a negative charge as V^{3+}, indicating the potential coexistence of different valence states of V ions in the semi-insulating samples. From another perspective, the position of the Fermi level in the system is pinned near the V(0/−) transition level within the bandgap. This is consistent with recent findings reported in Ref. 54, where the Fermi level of nominally n-type samples with V doping concentrations in the range of 10^{15}–10^{16} cm^{-3}, grown via CVD, was observed near the V acceptor level. Additionally, Ref. 55 also reported that in V-compensated semi-insulating samples with high V doping concentrations, the Fermi level is eventually pinned to the V acceptor level as the N concentration increases. These discussions confirm that the calculated (0/−) thermodynamic transition level, i.e., the V acceptor level, is reasonable.

Furthermore, we compared our results with theoretical calculations reported in several references, as shown in Fig. 3(a). Specifically, Miao and Lambrecht[22] provided calculated transition levels for V substitutional impurities at both cubic *k*- and hexagonal *h*-Si sublattice sites, while Prezzi *et al.*[23] presented transition levels for the *k*-site. Ivády *et al.*[43] and Huang *et al.*[56] reported calculated transition levels for $V_{Si}(h)$ at the (0/−) and (0/+) levels. It can be observed that our calculated (0/−) transition level is in close agreement with the results from Refs. 22 and 43. Similarly, our (0/+) transition level calculation is also consistent with the results reported in Ref. 22. The discrepancies between the calculated transition levels in these references may arise from the use of different pseudopotentials, exchange-correlation functionals, and image charge correction schemes. Overall, the use of the HSE + V_w method helps to correct the over-localization of defect states caused by standard HSE hybrid functionals, which often lead to overly deep defect energy levels. Moreover, the proper incorporation of image charge corrections avoids the underestimation of the formation energies of charged systems.

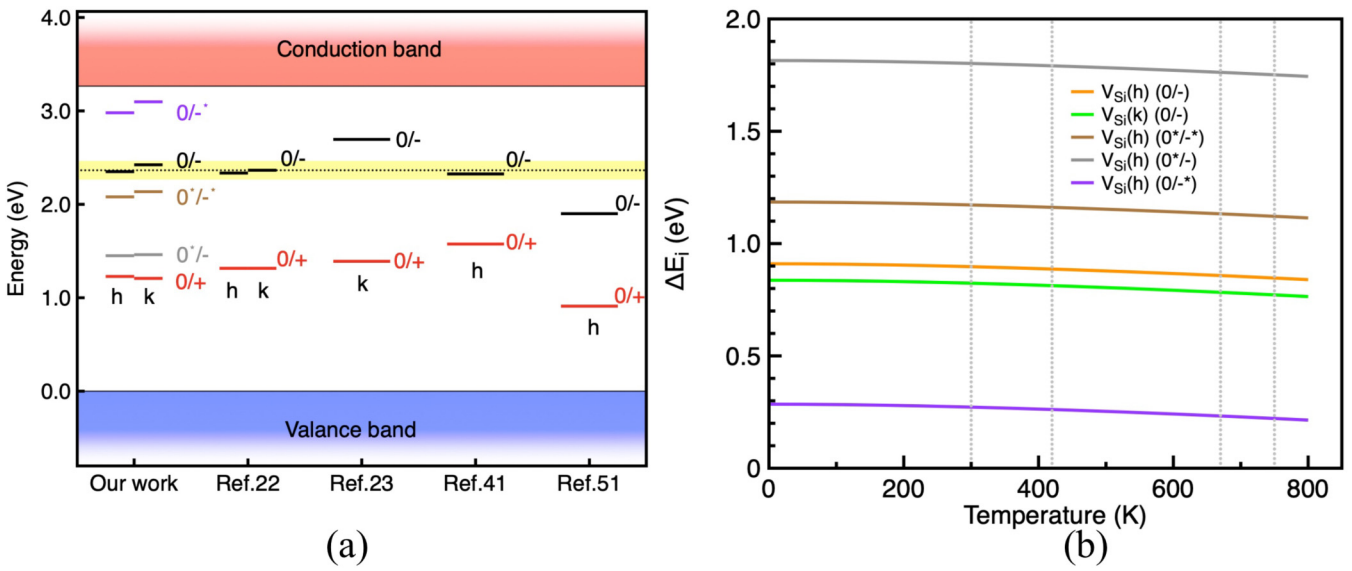

FIG. 3. (a) Comparison of the calculated transition level positions for V_{Si}(h) and V_{Si}(k) at 0 K in this study with the results from Refs. 22, 23, 43, and 56. Note that Ref. 23 only calculated the transition level positions for V impurities at the *k* site, while Refs. 43 and 56 only calculated the transition levels for V_{Si}(h). (b) Temperature dependence of the (0/−) transition levels (defect ionization energy ΔE_i in eV) for V_{Si}(h) and V_{Si}(k) from 0 to 800 K, taking into account the temperature-related band edge shifts and the quasiharmonic free energy differences between different charge states. The silver dotted lines in the figure correspond to temperatures of 300, 420, 670, and 750 K, respectively.

2. Energy levels associated with intra-shell transitions

When considering the intra-shell excited states of V substitutional impurities in different charge states, additional thermodynamic transition levels appear in the bandgap. For the neutral V^{4+} with $S = 1/2$ spin-singlet, Spindlberger *et al.*[14] reported zero-phonon line (ZPL) energies of 0.785 eV for the transition from the $^2A_1$ excited state to the ^2E ground state at the *h* site, and 0.845 eV for the transition from the ^2E excited state to the ^2E ground state at the *k* site. In this context, we disregard the energy level splitting caused by spin–orbit coupling, which corresponds to the emission energies of several hyperfine α and β lines in the PL spectrum. We also neglect higher-energy excited states. For the $S = 1$ spin-triplet V^{3+} with one negative charge, the cubic crystal field causes the free ion's ^3F state to split into a $^3A_2$ ground state and $^3T_2$ and $^3T_1$ excited states. According to Ref. 19, the ZPL energies for the lowest intra-3*d* shell transitions ($^3A_2 \rightarrow {}^3T_2$) of V^{3+} ions at *h* and *k* sites are 0.63 and 0.67 eV, respectively. Here, we again disregard the further splitting of the $^3T_2$ level due to spin–orbit coupling and higher-energy excited states such as $^3T_1$. It is noteworthy that these ZPL energy results were obtained through theoretical calculations using methods such as the delta-self-consistent-field method, analyzing experimental results from photoluminescence and electron paramagnetic resonance studies.

Figures 2(a) and 2(b) also include dashed lines representing the formation energy changes of excited states with respect to the Fermi level. The labels distinguishing different ground and excited states are positioned along the right vertical axis. As observed in the figure, for V substitutional impurities at both *h* and *k* sites, the intersections of the total energy lines (varying with the Fermi level) for different charge states, $S = 1$ and $S = 1/2$ ground and excited states, introduce three additional types of energy levels. Figure 3(a) illustrates the positions of these levels within the bandgap, labeled as (0*/−), (0/−*), and (0*/−*). Specifically, (0*/−) represents the thermodynamic transition level between the $^3A_2$ ground state of V^{3+} and the excited states ($^2A_1$ for the *h* site and ^2E for the *k* site) of V^{4+} at either *h* or *k* sites, (0/−*) denotes the thermodynamic transition level between the $^3T_2$ excited state of V^{3+} and the ^2E ground state of V^{4+} at either *h* or *k* sites, and (0*/−*) indicates the thermodynamic transition level between the $^3T_2$ excited state of V^{3+} and the excited states ($^2A_1$ for the *h* site and ^2E for the *k* site) of V^{4+} at either *h* or *k* sites.

As observed in Fig. 3(a), at 0 K, the (0*/−*) and (0*/−) transition levels are positioned lower in the bandgap than the (0/−) transition level, while the (0/−*) transition level is higher than the (0/−) level. Specifically, for V_{Si}(h), the (0*/−*) level is located at CBM − 1.18 eV, the (0*/−) level at CBM − 1.82 eV, and the (0/−*) transition level at CBM − 0.28 eV. For V_{Si}(k), these levels are positioned at CBM − 1.13, CBM − 1.80, and CBM − 0.17 eV, respectively.

B. The temperature dependence of the ionization energy

The thermodynamic transition level at the ground state, i.e., the ionization energy at 0 K, has been given above. To study the temperature dependence of the ionization energy, two effects mentioned in the literature[27,28] are considered in this section: the

temperature dependence of the band edges and the quasiharmonic free energy corresponding to defects with different charge states.

First, regarding the temperature dependence of the band edges for 4H-SiC, the literature points out that, compared to thermal expansion, which only minimally increases the lattice constants, electron–phonon interaction predominantly governs the thermal evolution of the band structure.[57] They not only confirmed that the value of the indirect bandgap determined via *ab initio* many-body perturbation theory aligns well with experimental results but also provided detailed insights into the temperature evolution of the band edges. Therefore, in this study, we fit the thermal evolution of the CBM and VBM as provided in Ref. 57 and consider the additional changes induced by this evolution when calculating the temperature dependence of the transition levels.

Second, for the quasiharmonic free energy corresponding to defects with different charge states, we divided the process into two steps. For example, for neutral or negatively charged $V_{Si}(h)$, we first calculate the phonon frequencies ω_i of the subsystem, where the subsystem refers to all atoms within a 2.4 Å radius surrounding the substitutional V atom. Subsequently, by applying the following statistical and mathematical transformations, specifically using the equation[58]

$$F^{qh} = \sum_i \left\{ \frac{\hbar\omega_i}{2} + k_B T \ln\left[1 - \exp\left(-\frac{\hbar\omega_i}{k_B T}\right)\right]\right\}, \tag{4}$$

the quasiharmonic free energy corresponding to the subsystem's phonon frequencies can be obtained. The temperature dependence of the transition levels is then calculated by considering the variation in the difference between the quasiharmonic free energy of defects with different charge states as a function of temperature. Figure 3(b) shows the temperature dependence of the (0/−) transition levels, i.e., the corresponding ionization energies (ΔE_i), for $V_{Si}(h)$ and $V_{Si}(k)$ over the temperature range of 0 ∼ 800 K, considering the two effects mentioned above. It can be observed that at the highest temperature of 800 K, the (0/−) transition levels for $V_{Si}(h)$ and $V_{Si}(k)$ decrease by 0.07 eV compared to the ground state. This variation falls within the error range of DLTS experiments and fitting, making it challenging to validate directly through experiments. However, as we will see, this temperature dependence plays a significant role in predicting the temperature dependence of the capture cross sections.

Figure 3(b) also illustrates the temperature dependence of the $(0^*/-)$, $(0/-^*)$, and $(0^*/-^*)$ transition levels, assuming that the intra-transition excited states do not alter the defect's local structure or corresponding phonon modes. Similar to the (0/−) transition level, at the maximum temperature of 800 K, the $(0^*/-)$, $(0/-^*)$, and $(0^*/-^*)$ transition levels for $V_{Si}(h)$ all decrease by 0.07 eV compared to their positions at 0 K.

C. The temperature dependence of the cross section

In calculating the temperature dependence of the capture cross section, we assume that the carrier capture process associated with the V_{Si} defect is nonradiative, i.e., it involves a multiphonon process related to electron–phonon coupling. Generally, in calculations, the nonradiative capture cross section σ_{ab} can be expressed as $\sigma_{ab} = C_{nonrad}/v_c$, where v_c is the thermal velocity of the captured carrier. In this study, we focus on the capture of conduction band electrons by neutral V impurities. For the thermal velocity, we adopt a value of 1.08×10^7 cm s^{-1} at 300 K, and for other temperatures, the thermal electron velocity is calculated based on this value. C_{nonrad} represents the nonradiative capture rate constant and can be expressed as $C_{nonrad} = R_{ab} \cdot V$, where V is the volume of the supercell (2.07×10^{-21} cm^3), and R_{ab} is the nonradiative capture rate. Under the harmonic approximation, R_{ab} can be written as[59]

$$R_{ab} = \frac{1}{\hbar}\left(\frac{\pi}{\lambda k T}\right)^{1/2}\left[kT\sum_l \frac{\left|\sum_i \langle a|\frac{\partial H}{\partial R_i}|b\rangle V_l(i)/\sqrt{m_i}\right|^2}{\omega_l^2}\right] e^{-(\Delta E_i-\lambda)^2/4\lambda k_B T}, \tag{5}$$

where a and b represent the initial and final electronic states, H denotes the Hamiltonian of the system, m_i is the nuclear mass, ω_l represents the phonon frequency, $V_l(i)$ is the normalized phonon mode vector for mode l and atom index i, and R_i is the coordinate of atom i. λ is the reorganization energy, T is the temperature, and ΔE_i is the ionization energy associated with the thermodynamic transition levels of the defects. Similarly to the calculation of the subsystem phonon frequencies, the phonon modes and frequencies associated with the defect were calculated using the combined dynamic matrix (CDM) method.[60] A truncation radius of 2.40 Å was employed to encompass the nearest neighboring atoms of the defect in all charge states. From Eq. (5), it can be seen that R_{ab} explicitly depends on the temperature T, and it also implicitly includes the temperature dependence of T through ΔE_i. Furthermore, when calculating σ_{ab} from R_{ab}, the temperature effect is introduced again through the expression for the thermal velocity of electrons $v_c = \sqrt{\frac{3k_B T}{m^*}}$, where m^* is the effective mass for electrons.

Figures 4(a) and 4(b) illustrate the variation of the electron capture cross section σ_{ab} of neutral $V_{Si}(h)$ and $V_{Si}(k)$ as a function of ΔE_i under four specific temperatures. First, it can be observed that at the same ΔE_i, the capture cross section increases with rising temperature, but the rate of increase slows down as the temperature further rises. Second, at a fixed temperature, the capture cross section decreases exponentially with increasing transition level, as described by Eq. (3). The positions of the transition levels at the corresponding temperatures are indicated by dashed lines, and the intersections with the solid lines represent the capture cross section values when the temperature dependence of the transition levels is considered. Specifically, at room temperature (300 K), the electron capture cross section of neutral $V_{Si}(h)$ is approximately 2.71×10^{-18} cm^2, which increases to 1.38×10^{-16} cm^2 at 420 K. For $V_{Si}(k)$, the electron capture cross section is 7.10×10^{-18} cm^2 at room temperature, slightly larger than that of neutral $V_{Si}(h)$, and increases to 1.79×10^{-16} at 420 K, also slightly larger than that of neutral $V_{Si}(h)$. The shaded regions in the figure represent the variation range of the transition energy levels from 0 to 750 K. It is evident that the temperature-dependent variation of the transition levels significantly influences the determination of the capture cross section, with this effect being more pronounced at lower temperatures. For instance, in the case of neutral $V_{Si}(h)$, the difference between the upper and lower bounds of the transition levels at 300 K leads to a tenfold variation in the capture cross section.

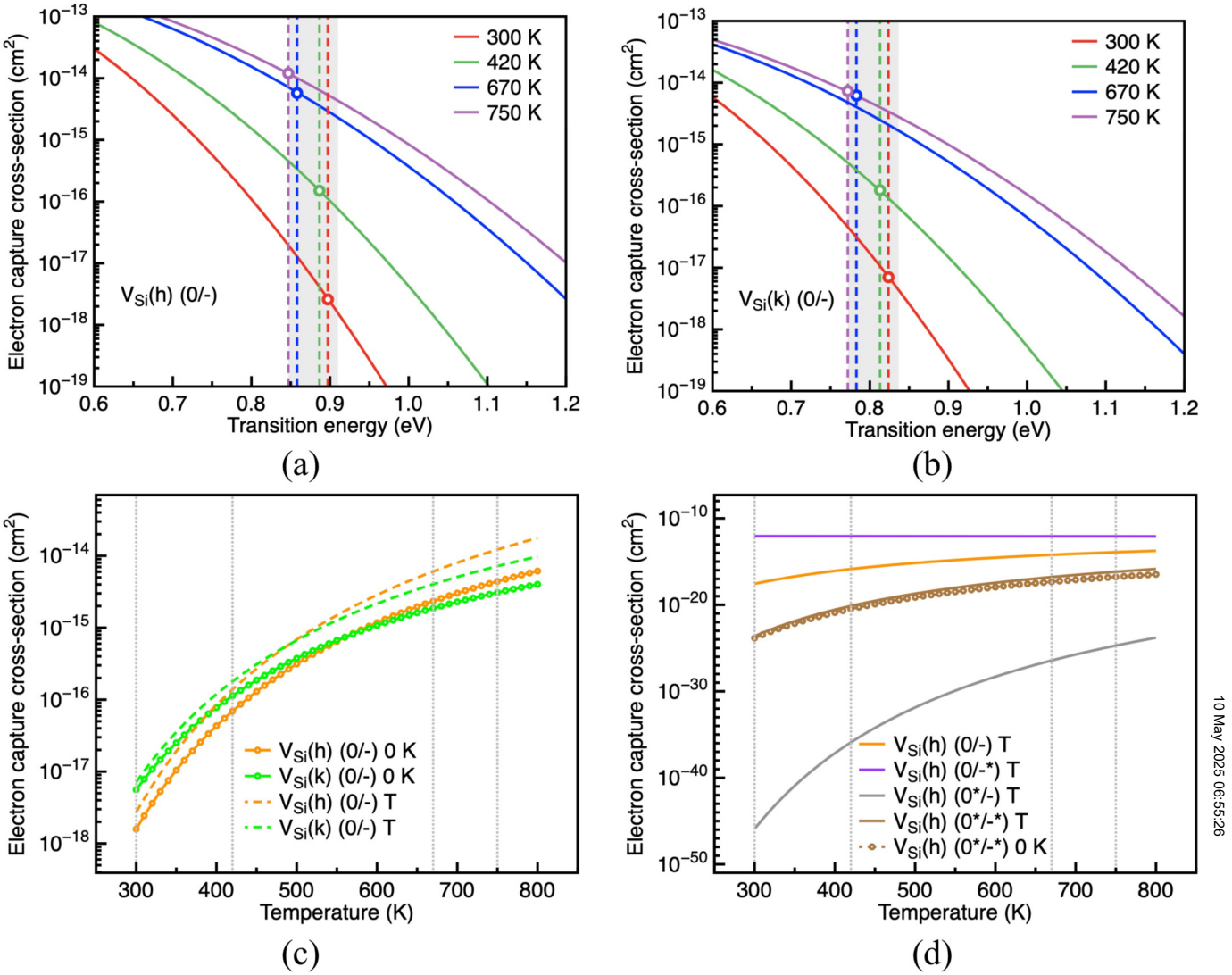

FIG. 4. (a) Electron capture cross sections σ_{ab} of neutral V_{Si}(h) as a function of ionization energy ΔE_i at 300, 420, 670, and 750 K. (b) Electron capture cross sections σ_{ab} of neutral V_{Si}(k) as a function of ionization energy ΔE_i at 300, 420, 670, and 750 K. (c) Temperature dependence of electron capture cross sections for neutral V_{Si}(h) (orange) and V_{Si}(k) (green) defects. Solid lines and hollow points represent calculations using ionization energies at 0 K, while dashed lines represent calculations using temperature-dependent ionization energies. (d) Temperature dependence of capture cross sections for V_{Si}(h) corresponding to (0*/−), (0/−*), and (0*/−*) transition levels, calculated using temperature-dependent ionization energies. These are represented by gray, purple, and brown solid lines, respectively. The orange solid line represents the capture cross section for the V_{Si}(h) (0/−) transition level for comparison. Additionally, the temperature dependence of electron capture cross sections calculated using 0 K ionization energies is included for comparison, shown as brown hollow points and dashed lines. Furthermore, in (a) and (b), the intersections between the dashed lines (representing transition energy level positions) and solid lines (indicating capture cross sections) are marked, while in (c) and (d), silver dotted lines denote temperatures of 300, 420, 670, and 750 K.

For neutral V_{Si}(k), the difference in the transition levels at 750 K results in approximately a 2.5-fold variation in the capture cross section.

Figure 4(c) further illustrates the temperature dependence of electron capture cross sections for neutral V_{Si}(h) and V_{Si}(k) defects, calculated using ionization energies at 0 K and temperature-dependent ionization energies. Generally, for both defects, the capture cross sections computed using temperature-dependent ionization energies are higher than those calculated using ground state ionization energies. For instance, at 750 K, the former is 2.77 times higher than the latter for neutral V_{Si}(h), further confirming the impact of temperature-dependent transition levels. Additionally, it can be observed that at room temperature, the electron capture cross section of V impurities at cubic Si sublattice sites is larger than that

of V impurities at hexagonal Si sublattice sites. However, as the temperature increases to 500 K, this relationship inverts. When using actual temperature-dependent ionization energies for calculations, this transition temperature is lower than the corresponding temperature of 560 K obtained using 0 K ionization energies. Finally, using the $V_{Si}(k)$ defect as an example (calculated with temperature-dependent ionization energies), the capture cross section at 420 K is about 25 times that at 300 K. This ratio increases to 568 at 670 K, and ultimately, the capture cross section at 750 K is approximately 1000 times that at room temperature. This demonstrates that the real capture cross section increases rapidly with rising temperature.

Now, let us consider the temperature dependence of the capture cross section corresponding to the transition energy levels introduced by intra-transition excited states, as shown in Fig. 4(d). Due to the differing positions of the excited-state-associated transition levels compared to the 0/− transition level, their corresponding capture cross sections exhibit significant variations. At room temperature, the capture cross section for the $V_{Si}(h)$ $(0^*/-)$ transition level is 1.24×10^{-46} cm^2, substantially smaller than that of $V_{Si}(h)$ (0/−). Similarly, the capture cross section for the $(0^*/-^*)$ transition level is 2.36×10^{-24} cm^2, also smaller than the $V_{Si}(h)$ (0/−) value. However, the capture cross section for the $(0/-^*)$ transition level at 300 K is 8.68×10^{-13} cm^2, approximately 3.2×10^5 times larger than that of (0/−) at the same temperature. This demonstrates that the capture cross sections of excited-state-associated transition levels indeed differ significantly from the (0/−) transition level at room temperature. As the temperature increases from 300 to 800 K, the capture cross section of the $(0^*/-)$ transition level changes from 1.24×10^{-46} to 1.58×10^{-24} cm^2, showing a more pronounced increase compared to (0/−). The $(0^*/-^*)$ transition level exhibits a slightly smaller change with temperature, increasing from 2.36×10^{-24} cm^2 at 300 K to 1.42×10^{-16} cm^2 at 800 K. Interestingly, the $(0/-^*)$ transition level shows an opposite trend, slightly decreasing from 8.68×10^{-13} to 8.18×10^{-13} cm^2 as the temperature rises.

The differing temperature trends in capture cross sections can be attributed to the exponential term $e^{-(\Delta E_i-\lambda)^2/4\lambda k_B T}$ in Eq. (2), which involves the difference between the transition level and the reorganization energy. Assuming no changes in the defect's local structure due to intra-transition excited states, the reorganization energy is taken as a constant 0.28 eV for all cases. The $(0/-^*)$ level at 0 K coincides with this value, resulting in the capture cross section approaching its maximum at low temperatures. As shown in Fig. 3(b), with increasing temperature, the ionization energy ΔE_i for the $(0/-^*)$ level gradually decreases, causing it to deviate more from the reorganization energy and leading to a decrease in the capture cross section. For the other three transition levels, which are higher than the reorganization energy at low temperatures, the transition levels decrease as temperature rises, bringing them closer to the reorganization energy. This ultimately results in an exponential increase in their capture cross sections.

D. Interpretation of DLTS experimental data for V-doped 4H-SiC

In this section, we present the characterization data from DLTS experiments and attempt to interpret the Arrhenius fitting results based on theoretical calculations. Figure 5 shows the I-DLTS spectra of V-doped 4H-SiC semi-insulating samples in dark conditions for low-temperatures (320–460 K) (a) and high-temperatures (600–760 K) (b) regions, respectively. In Fig. 5(a), a significant DLTS signal peak, labeled E1, is observed around 425 K. By performing an Arrhenius fitting on the E1 peak using the deep level transient Fourier spectroscopy (DLTFS) method, an activation energy of 0.85 eV and an apparent capture cross section of 1.30×10^{-14} cm^2 were obtained, with a correlation coefficient greater than 0.997, as shown in Fig. 5(c). Furthermore, based on the same dataset, the fitting method employing high energy resolution energy analysis (HERA) evaluation yielded an activation energy of 0.88 eV and an apparent capture cross section of 1.28×10^{-14} cm^2, while maintaining a correlation coefficient greater than 0.995. It can be observed that, despite the different data fitting methods, the activation energy and capture cross section obtained using the HERA method differ from those obtained using the DLTFS method by approximately 3.5% and 1.5%, respectively, indicating a relatively low level of uncertainty.

This activation energy value for the vanadium acceptor level is consistent with earlier reports: 0.82 eV by Lauer *et al.*,[24] 0.88 ∼ 0.97 eV by Dalibor *et al.*,[25] and 0.80 eV by Jenny *et al.*[26] Recently, electron-active deep levels in V-doped semi-insulating SiC were also investigated using I-DLTS, reporting an energy level of 0.87 eV possibly related to the V_{Si} defect.[17] Our characterization results are also close to their reported value. These experimental findings correspond well with the average of the (0/−) transition levels for $V_{Si}(h)$ and $V_{Si}(k)$ at 425 K, which are 0.89 eV and 0.81 eV, respectively, as shown in Fig. 3(b). This agreement indicates that our theoretical calculations effectively explain the experimental DLTS spectral results.

In terms of capture cross section measurements, Lauer *et al.*[24] and Jenny *et al.*[26] reported values of 1.79×10^{-16} and 2×10^{-16} cm^2, respectively. These results are consistent with our theoretical calculation result of 1.40×10^{-16} cm^2 at 420 K, as shown in Fig. 4. However, this result differs significantly from the apparent capture cross section measured in our experiment. The capture cross section in the aforementioned earlier experiments was obtained using capacitance-mode DLTS (C-DLTS) characterization. For our high-resistivity samples, it is challenging to resolve signals using the capacitance mode, because acquisition of capacitance signals requires electrical conduction outside of the space charge region. In contrast, our test data were obtained using I-DLTS measurements. The differences between current-mode and capacitance-mode DLTS may lead to inaccuracies in the capture cross section fitting. Booker *et al.*[31] investigated the ON deep level in 4H-SiC using multiple high-resolution capacitance deep-level transient spectroscopy spectra measured with different filling-pulse lengths. They pointed out that, while the deviation in enthalpy (transition energy level) values obtained from sample to sample and across different measurement batches is about 2%, the error in the capture cross section can reach up to 30%. Similarly, Bathen *et al.*[61] reported an uncertainty of up to an order of magnitude for the capture cross section of boron-related defects in 4H-SiC based on minority carrier transient spectroscopy. Therefore, considering the above comparisons, the uncertainty in our capture cross section measurements based on I-DLTS is expected to exceed an order of magnitude.

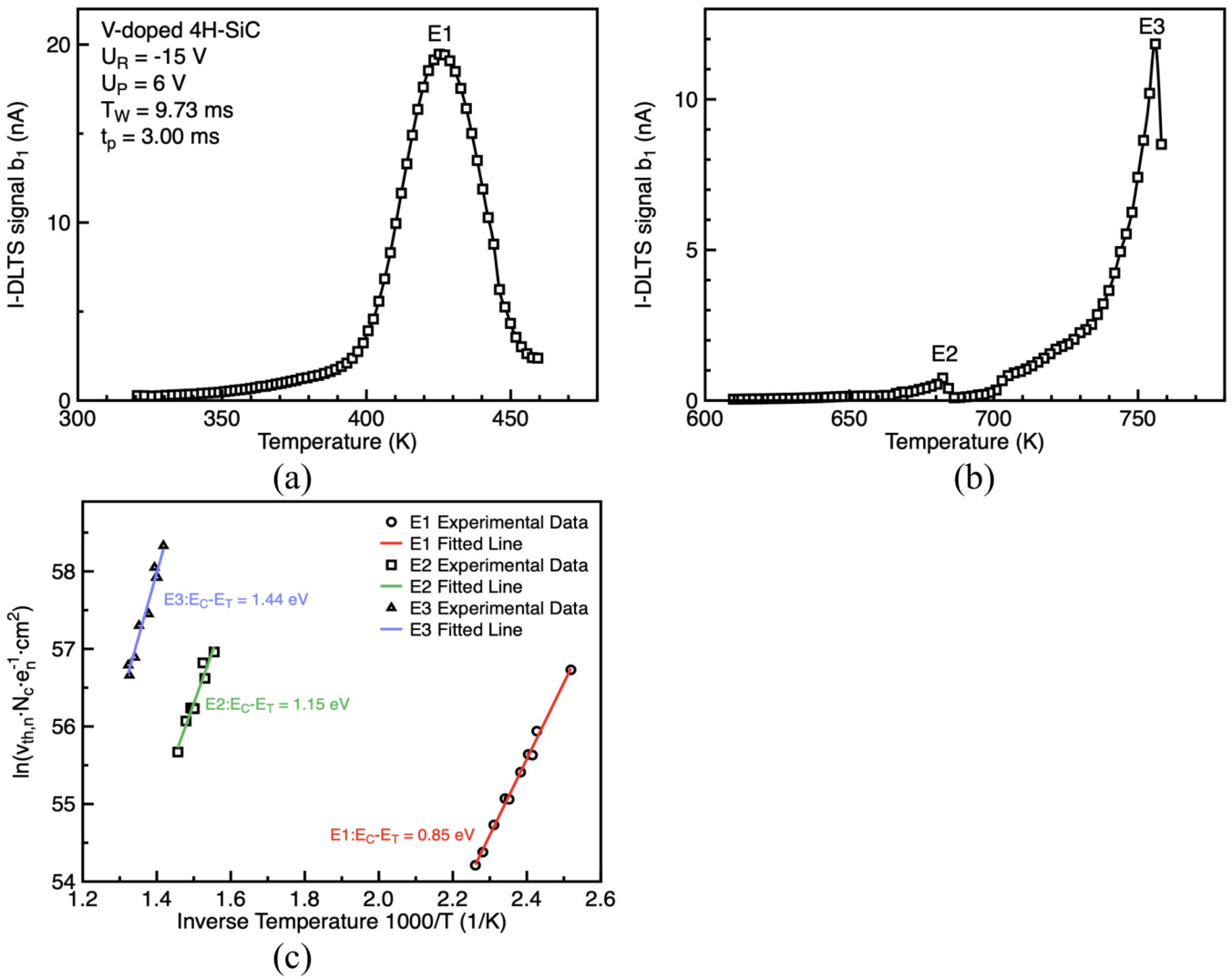

FIG. 5. I-DLTS spectra and Arrhenius plot of V-doped 4H-SiC semi-insulating samples under dark conditions. (a) I-DLTS spectrum in the low-temperature range (320–460 K). A prominent DLTS signal peak, labeled as E1, is observed at approximately 425 K. (b) I-DLTS spectrum in the high-temperature range (600–760 K). Two peaks, labeled as E2 and E3, are observed at approximately 660 and 750 K, respectively. (c) Arrhenius fitting plot for the E1, E2, and E3 peaks. The activation energies and apparent cross sections derived from this plot are presented in Table I.

Additionally, as mentioned above, the failure to separate the entropy factor from the apparent capture cross section obtained through Arrhenius fitting may also lead to an overestimation of the latter. Notably, if the measurement uncertainty of the apparent capture cross section is incorporated into the calculation of the entropy factor, a comparison between the experimentally obtained apparent capture cross section of $1.30 \times 10^{-14}\,\mathrm{cm}^2$ from I-DLTS and the theoretically calculated capture cross section of $1.40 \times 10^{-16}\,\mathrm{cm}^2$ yields an entropy factor ΔS of approximately $4.53\,k_B$, as shown in Table I. This value is slightly larger than that of the $Z_{1/2}$ level associated with carbon vacancy defects in 4H-SiC, as mentioned in Sec. I, but smaller than the value corresponding to the D1 level related to deep B impurities. Finally, a small portion of the observed discrepancy may also originate from the theoretical value itself. This is because our calculation only considers nonradiative carrier capture based on the multiphonon emission (MPE) process. However, recent studies have suggested that trap-assisted Auger–Meitner (TAAM) carrier capture may also play a role in nonradiative losses in wide-bandgap semiconductors.

In the high-temperature region I-DLTS signal shown in Fig. 5(b), two peaks, E2 and E3, can be observed at approximately 660 and 750 K, respectively. Arrhenius fitting of the E2 and E3 peaks yields activation energies of 1.15 and 1.44 eV, and apparent capture cross sections of 1.75×10^{-16} and $1.03 \times 10^{-15}\,\mathrm{cm}^2$,

TABLE I. Activation energies and apparent capture cross sections for the E1, E2, and E3 levels, obtained through Arrhenius fitting of each peak. Also presented are the computed ionization energies and corresponding theoretical capture cross sections for the possible V_{Si}(h,k) (0/−) and V_{Si}(h,k) (0*/−*) transition levels associated with E1 and E2 at the respective measurement temperatures. The entropy factors for E1 and E2 were derived by combining theoretically calculated and DLTS-characterized apparent capture cross sections, incorporating the measurement uncertainties of the apparent capture cross section.

Deep level	E1	E2	E3
Activation energy (eV)	0.85	1.15	1.44
Ionization energy (eV)	0.87, 0.81	1.16, 1.11	…
Apparent cross section (cm^2)	1.30×10^{-14}	1.75×10^{-16}	1.03×10^{-15}
Calculated cross section (cm^2)	1.40×10^{-16}, 1.79×10^{-16}	1.33×10^{-17}, 3.78×10^{-17}	…
Entropy factor (k_B)	4.53, 4.28	2.58, 1.53	…

respectively, as shown in Table I. The temperature-dependent ionization energy plot in Fig. 3(b) indicates that the V_{Si}(h) (0*/−*) transition level at 660 K has a ΔE_i of approximately 1.13 eV, which is consistent with the activation energy corresponding to the E2 peak. The ON2 defect observed in Ref. 31 is located at a position close to this energy level. However, this defect typically appears in n-type 4H-SiC after high-temperature oxidation, a process our test samples have not undergone. Figure 4 shows that the theoretically calculated capture cross section at 660 K is approximately 1.33×10^{-17} cm^2. Assuming this value as the true capture cross section, the calculated ΔS related to the entropy factor is 2.58 k_B, which is lower compared to the (0/−) transition level. This reduction might be attributed to our neglect of defect local structure changes caused by intra-transition excited states in the theoretical capture cross section calculations. The E3 peak can be assigned to the UT1 defect, as reported in previous literature.[62]

IV. CONCLUSION

We employed first-principles calculations based on density functional theory to investigate the temperature-dependent (0/−) transition levels of V dopants at hexagonal and cubic Si sites in 4H-SiC. Our calculations reveal that these transition levels decrease by approximately 0.07 eV at 800 K compared to 0 K. We calculated the temperature dependence of electron capture cross sections for V-doped defects. The results show a significant increase in capture cross sections with rising temperature, with V_{Si}(k) reaching up to about 1000 times its room temperature value at 750 K. Considering the intra-transition excited states of V defects, we predicted additional transition levels (0*/−, 0/−*, 0*/−*) and their corresponding capture cross sections. These additional levels exhibit substantial differences in capture cross sections compared to the (0/−) level at room temperature. Current-mode DLTS characterization was performed on V-doped 4H-SiC samples. A primary peak E1 was observed near 425 K, with an activation energy of 0.85 eV, aligning well with the theoretically calculated (0/−) transition level. Two additional peaks, E2 and E3, were observed in the high-temperature region. The activation energy of the E2 peak, appearing at 660 K, is consistent with our theoretical calculations of the V_{Si}(h) (0*/−*) level. Furthermore, we discussed the discrepancies between the theoretically calculated capture cross sections and the apparent capture cross sections obtained from DLTS measurements and calculated the entropy factor.

In conclusion, we comprehensively investigated the effects of temperature and intra-3*d* shell transitions on the position of V acceptor impurity transition levels within the bandgap of 4H-SiC and their corresponding capture cross sections using density functional theory calculations. This provides a new approach for in-depth understanding of defect levels in V-doped 4H-SiC and their corresponding DLTS signals, while also offering a theoretical basis for studying the optical and electrical properties of related power and quantum devices.

ACKNOWLEDGMENTS

This work was supported by the National Natural Science Foundation of China (NNSFC) (Grant Nos. 62004153, 62104186, and 62474139) and the Natural Science Basic Research Program of Shaanxi (No. 2024JC-YBMS-474). B.P. expresses special thanks to Beijing Lonxun Quantum Company for their guidance.

AUTHOR DECLARATIONS

Conflict of Interest

The authors have no conflicts to disclose.

Author Contributions

Yuxuan Lan: Conceptualization (equal); Data curation (equal); Formal analysis (supporting); Writing – original draft (supporting); Writing – review & editing (supporting). **Bo Peng:** Conceptualization (lead); Data curation (equal); Formal analysis (equal); Funding acquisition (equal); Writing – original draft (lead); Writing – review & editing (equal). **Yutian Wang:** Data curation (supporting); Funding acquisition (equal); Software (supporting); Writing – review & editing (supporting). **Hao Yuan:** Funding acquisition (supporting); Methodology (supporting); Resources (supporting). **Jichao Hu:** Methodology (supporting); Software (supporting); Supervision (supporting). **Linpeng Dong:** Funding acquisition (supporting); Resources (supporting). **Hui Guo:** Funding acquisition (equal); Resources (supporting). **Yuming Zhang:** Funding acquisition (equal); Project administration (equal); Resources (supporting).

DATA AVAILABILITY

The data that support the findings of this study are available from the corresponding author upon reasonable request.

REFERENCES

[1]T. Kimoto and J. A. Cooper, *Fundamentals of Silicon Carbide Technology: Growth, Characterization, Devices and Applications* (John Wiley & Sons, 2014).
[2]C. Langpoklakpam, A.-C. Liu, K.-H. Chu, L.-H. Hsu, W.-C. Lee, S.-C. Chen, C.-W. Sun, M.-H. Shih, K.-Y. Lee, and H.-C. Kuo, "Review of silicon carbide processing for power MOSFET," Crystals **12**, 245 (2022).
[3]N. J. Kramer, L. F. Voss, A. M. Conway, P. V. Grivickas, M. Bora, D. L. Hall, and A. N. Caruso, "Extrinsic absorption pathways in vanadium-doped SiC

measured using a total internal reflection geometry," Phys. Stat. Sol. A **217**, 2000315 (2020).
[4]T. Miyazawa, T. Tawara, R. Takanashi, and H. Tsuchida, "Vanadium doping in 4H-SiC epitaxial growth for carrier lifetime control," Appl. Phys. Express **9**, 111301 (2016).
[5]W. C. Mitchel, W. D. Mitchell, G. Landis, H. E. Smith, W. Lee, and M. E. Zvanut, "Vanadium donor and acceptor levels in semi-insulating 4H- and 6H-SiC," J. Appl. Phys. **101**, 013707 (2007).
[6]N. T. Son, P. Carlsson, A. Gällström, B. Magnusson, and E. Janzén, "Deep levels and carrier compensation in V-doped semi-insulating 4H-SiC," Appl. Phys. Lett. **91**, 202111 (2007).
[7]Q. Sun, H. Guo, Z. Zheng, F. Zhang, F. Hong, Y. Zhang, Y. Wang, and S. Jiang, "Influence of pinch effect on the lifetime of a 2 MW silicon carbide photoconductive semiconductor switch," IEEE Trans. Electron Devices **71**, 2018–2023 (2024).
[8]T. He, T. Shu, H. Yang, M. Yi, F. Liu, J. Yao, L. Wang, and T. Xun, "Effect of donor–acceptor compensation on transient performance of vanadium-doped SiC photoconductive switches using 532-nm laser," IEEE Trans. Electron Devices **71**, 4275–4282 (2024).
[9]X. Chu, T. Xun, L. Wang, H. Yang, J. Liu, J. He, and J. Zhang, "Wide-range frequency-agile microwave generation up to 10 GHz based on vanadium-compensated 4H-SiC photoconductive semiconductor switch," IEEE Electron Device Lett. **43**, 1013–1016 (2022).
[10]T. Astner, P. Koller, C. M. Gilardoni, J. Hendriks, N. Tien Son, I. G. Ivanov, J. Ul Hassan, C. H. van der Wal, and M. Trupke, "Vanadium in silicon carbide: Telecom-ready spin centres with long relaxation lifetimes and hyperfine-resolved optical transitions," Quant. Sci. Technol. **9**, 035038 (2024).
[11]J. Ahn, C. Wicker, N. Bitner, M. T. Solomon, B. Tissot, G. Burkard, A. M. Dibos, J. Zhang, F. J. Heremans, and D. D. Awschalom, "Extended spin relaxation times of optically addressed vanadium defects in silicon carbide at telecommunication frequencies," Phys. Rev. Appl. **22**, 044078 (2024).
[12]G. Wolfowicz, C. P. Anderson, B. Diler, O. G. Poluektov, F. J. Heremans, and D. D. Awschalom, "Vanadium spin qubits as telecom quantum emitters in silicon carbide," Sci. Adv. **6**, eaaz1192 (2022).
[13]B. Tissot, M. Trupke, P. Koller, T. Astner, and G. Burkard, "Nuclear spin quantum memory in silicon carbide," Phys. Rev. Res. **4**, 033107 (2022).
[14]L. Spindlberger, A. Csóré, G. Thiering, S. Putz, R. Karhu, J. Hassan, N. Son, T. Fromherz, A. Gali, and M. Trupke, "Optical properties of vanadium in 4H silicon carbide for quantum technology," Phys. Rev. Appl. **12**, 014015 (2019).
[15]A. Chakravorty and D. Kabiraj, "Role of Fermi-level depinning in quenching of V^{4+} related photoluminescence in semi-insulating 4H-SiC," Semicond. Sci. Technol. **37**, 095024 (2022).
[16]A. B. Renz, O. J. Vavasour, M. Rommel, G. Baker, P. M. Gammon, T. X. Dai, F. Li, M. Antoniou, P. A. Mawby, and V. A. Shah, "A study of high resistivity semi-insulating 4H-SiC epilayers formed via the implantation of germanium and vanadium," Mater. Sci. Forum **1062**, 523–527 (2022).
[17]G. Alfieri, L. Kranz, and A. Mihaila, "Current-mode deep level spectroscopy of vanadium-doped HPSI 4H-SiC," Mater. Sci. Forum **1004**, 331–336 (2020).
[18]K. Murata, T. Tawara, A. Yang, R. Takanashi, T. Miyazawa, and H. Tsuchida, "Wide-ranging control of carrier lifetimes in n-type 4H-SiC epilayer by intentional vanadium doping," J. Appl. Phys. **126**, 045711 (2019).
[19]H. J. von Bardeleben, S. A. Zargaleh, J. L. Cantin, W. B. Gao, T. Biktagirov, and U. Gerstmann, "Transition metal qubits in 4*H*-silicon carbide: A correlated EPR and DFT study of the spin $S = 1$ vanadium V^{3+} center," Phys. Rev. Mater. **3**, 124605 (2019).
[20]E. V. Edinach, A. D. Krivoruchko, A. S. Gurin, M. V. Muzafarova, I. V. Ilyin, R. A. Babunts, N. G. Romanov, A. G. Badalyan, and P. G. Baranov, "Application of high-frequency EPR spectroscopy for the identification and separation of nitrogen and vanadium sites in silicon carbide crystals and heterostructures," Semiconductors **54**, 150–156 (2020).
[21]M. Zvanut, W. Lee, W. Mitchel, W. Mitchell, and G. Landis, "The acceptor level for vanadium in 4H and 6H SiC," Phys. B **376–377**, 346–349 (2006).
[22]M. S. Miao and W. R. L. Lambrecht, "Electronic structure and magnetic properties of transition-metal-doped 3C and 4H silicon carbide," Phys. Rev. B **74**, 235218 (2006).
[23]D. Prezzi, T. A. G. Eberlein, J.-S. Filhol, R. Jones, M. J. Shaw, P. R. Briddon, and S. Öberg, "Optical and electrical properties of vanadium and erbium in 4H-SiC," Phys. Rev. B **69**, 193202 (2004).
[24]V. Lauer, G. Brémond, A. Souifi, G. Guillot, K. Chourou, M. Anikin, R. Madar, B. Clerjaud, and C. Naud, "Electrical and optical characterisation of vanadium in 4H and 6H-SiC," Mater. Sci. Eng. B **61–62**, 248–252 (1999).
[25]T. Dalibor, G. Pensl, H. Matsunami, T. Kimoto, W. J. Choyke, A. Schöner, and N. Nordell, "Deep defect centers in silicon carbide monitored with deep level transient spectroscopy," Phys. Stat. Sol. A **162**, 199–225 (1997).
[26]J. R. Jenny, J. Skowronski, W. C. Mitchel, H. M. Hobgood, R. C. Glass, G. Augustine, and R. H. Hopkins, "Deep level transient spectroscopic and Hall effect investigation of the position of the vanadium acceptor level in 4H and 6H SiC," Appl. Phys. Lett. **68**, 1963–1965 (1996).
[27]D. Wickramaratne, C. E. Dreyer, B. Monserrat, J.-X. Shen, J. L. Lyons, A. Alkauskas, and C. G. Van de Walle, "Defect identification based on first-principles calculations for deep level transient spectroscopy," Appl. Phys. Lett. **113**, 192106 (2018).
[28]X. Xu, X. Yu, J. Yang, T. Ying, X. Cui, Y. Jing, G. Lv, Z. Liu, W. Li, and X. Li, "To define nonradiative defects in semiconductors: An accurate DLTS simulation based on first-principle," Comput. Mater. Sci. **215**, 111760 (2022).
[29]L. Shi, K. Xu, and L.-W. Wang, "Comparative study of *ab initio* nonradiative recombination rate calculations under different formalisms," Phys. Rev. B **91**, 205315 (2015).
[30]R. Kassing, L. Cohausz, P. van Staa, W. Mackert, and H. J. Hoffman, "Determination of the entropy-factor of the gold donor level in silicon by resistivity and DLTS measurements," Appl. Phys. A **34**, 41–47 (1984).
[31]I. D. Booker, H. Abdalla, J. Hassan, R. Karhu, L. Lilja, E. Janzén, and E. Ö. Sveinbjörnsson, "Oxidation-induced deep levels in *n*- and *p*-type 4*H*- and 6*H*-SiC and their influence on carrier lifetime," Phys. Rev. Appl. **6**, 014010 (2016).
[32]S. A. Reshanov, G. Pensl, K. Danno, T. Kimoto, and S. Hishiki, "Effect of the Schottky barrier height on the detection of midgap levels in 4*H*-SiC by deep level transient spectroscopy," J. Appl. Phys. **102**, 113702 (2007).
[33]H. M. Ayedh, V. Bobal, R. Nipoti, A. Hallén, and B. G. Svensson, "Formation of carbon vacancy in 4H silicon carbide during high-temperature processing," J. Appl. Phys. **115**, 012005 (2014).
[34]O. Samperi, L. Vines, A. Hallén, and M. E. Fragalà, "Charge carrier capture by prominent defect centers in 4H-SiC," Def. Diffus. Forum **434**, 173–182 (2024).
[35]D. Wickramaratne, J.-X. Shen, C. E. Dreyer, M. Engel, and M. Marsman, "Iron as a source of efficient Shockley–Read–Hall recombination in GaN," Appl. Phys. Lett. **109**, 162107 (2016).
[36]W. Jia, J. Fu, Z. Cao, L. Wang, X. Chi, W. Gao, and L.-W. Wang, "Fast plane wave density functional theory molecular dynamics calculations on multi-GPU machines," J. Comput. Phys. **251**, 102–115 (2013).
[37]D. R. Hamann, "Optimized norm-conserving Vanderbilt pseudopotentials," Phys. Rev. B **88**, 085117 (2013).
[38]J. Heyd, G. E. Scuseria, and M. Ernzerhof, "Hybrid functionals based on a screened Coulomb potential," J. Chem. Phys. **118**, 8207–8215 (2003).
[39]J. P. Perdew, K. Burke, and M. Ernzerhof, "Generalized gradient approximation made simple," Phys. Rev. Lett. **77**, 3865–3868 (1996).
[40]W. Setyawan and S. Curtarolo, "High-throughput electronic band structure calculations: Challenges and tools," Comput. Mater. Sci. **49**, 299–312 (2010).
[41]L. Lin, K. Xie, and C. He, "Nitrogen-vacancy-modulated efficient ammonia desorption over 3d TM-anchored BC_3 N_2 monolayer," Phys. Chem. Chem. Phys. **26**, 2082–2092 (2024).
[42]P. Shi, D. Pang, Z. Zhang, L. Lin, and C. He, "Transition metals embedded Pt (1 0 0) surface as an electrocatalysts for no reduction reaction: A first-principles study," Appl. Surf. Sci. **619**, 156744 (2023).
[43]V. Ivády, I. A. Abrikosov, E. Janzén, and A. Gali, "Role of screening in the density functional applied to transition-metal defects in semiconductors," Phys. Rev. B **87**(20), 205201 (2013).

[44]Z.-J. Suo, J.-W. Luo, S.-S. Li, and L.-W. Wang, "Image charge interaction correction in charged-defect calculations," Phys. Rev. B **102**, 174110 (2020).
[45]B. Peng, M. Yu, K. Sun, L. Yuan, and Y. Zhang, "Advancing understanding of structural, electronic, and magnetic properties in 3d-transition-metal TM-doped α-Ga_2O_3 (TM = V, Cr, Mn, and Fe): A first-principles and Monte Carlo study," J. Appl. Phys. **134**, 225702 (2023).
[46]C. Freysoldt, B. Grabowski, T. Hickel, J. Neugebauer, G. Kresse, A. Janotti, and C. G. Van de Walle, "First-principles calculations for point defects in solids," Rev. Mod. Phys. **86**, 253–305 (2014).
[47]S.-H. Wei, "Overcoming the doping bottleneck in semiconductors," Comput. Mater. Sci. **30**, 337–348 (2004).
[48]L. Lin, T. Liu, Z. Zhang, H. Tao, M. He, B. Song, and Z. Zhang, "Vacancy induced magnetism in N-doped 4H-SiC by first-principle calculations," Solid State Sci. **49**, 78–82 (2015).
[49]D. R. Lide, *CRC Handbook of Chemistry and Physics* (CRC Press, 2004), 839–897. Vol. 85, pp.
[50]L. Lin, X. Yang, P. Shi, L. Yan, K. Xie, C. Deng, and Z. Chen, "Probing the origin of transition metal carbide VC for oxygen reduction reaction: A DFT study," Surf. Interfaces **40**, 103100 (2023).
[51]L. Lin, L. Yan, J. Huang, H. Tao, J. Zhang, W. Yu, and Y. Xu, "First-principles investigations of the effect of V and Fe dopants on the magnetic and optical properties of 4H-SiC," Thin Solid Films **709**, 138182 (2020).
[52]T. S. Wolfe, R. M. Van Ginhoven, and A. Strachan, "Computational study of first-row transition metals in monodoped 4H-SiC," Modell. Simul. Mater. Sci. Eng. **29**, 055008 (2021).
[53]K. Kojima, S.-I. Sato, T. Ohshima, and S.-I. Kuroki, "Growth of vanadium doped semi-insulating 4H-SiC epilayer with ultrahigh-resistivity," J. Appl. Phys. **131**, 245107 (2022).
[54]R. Karhu, E. Ö. Sveinbjörnsson, B. Magnusson, I. G. Ivanov, Ö. Danielsson, and J. Ul Hassan, "CVD growth and properties of on-axis vanadium doped semi-insulating 4H-SiC epilayers," J. Appl. Phys. **125**, 045702 (2019).
[55]W. Fu, L. Wang, B. Wang, X. Chu, T. Xun, and H. Yang, "Investigation on the photocurrent tail of vanadium-compensated 4H-SiC for microwave application," AIP Adv. **12**, 095121 (2022).
[56]Y. Huang, R. Wang, D. Yang, and X. Pi, "Impurities in 4H silicon carbide: Site preference, lattice distortion, solubility, and charge transition levels," J. Appl. Phys. **135**, 195703 (2024).
[57]E. Cannuccia and A. Gali, "Thermal evolution of silicon carbide electronic bands," Phys. Rev. Mater. **4**, 014601 (2020).
[58]D. C. Wallace, *Thermodynamics of Crystals* (Dover, New York, 1998).
[59]H.-S. Zhang, J. Gong, and L. Shi, "Antisite defect Si C as a source of the D center in 4H-SiC," Phys. Stat. Sol. **17**, 2200239 (2023).
[60]L. Shi and L.-W. Wang, "*Ab initio* calculations of deep-level carrier nonradiative recombination rates in bulk semiconductors," Phys. Rev. Lett. **109**, 245501 (2012).
[61]M. E. Bathen, P. Kumar, M. Ghezellou, M. Belanche, L. Vines, J. Ul-Hassan, and U. Grossner, "Dual configuration of shallow acceptor levels in 4H-SiC," Mater. Sci. Semicond. Process. **177**, 108360 (2024).
[62]K. Danno, T. Hori, and T. Kimoto, "Impacts of growth parameters on deep levels in n-type 4H-SiC," J. Appl. Phys. **101**, 053709 (2007).